npj | Quantum Materials

www.nature.com/npjquantmats

ARTICLE OPEN

Quasistatic antiferromagnetism in the quantum wells of $SmTiO_3/SrTiO_3$ heterostructures

Ryan F. Need[1], Patrick B. Marshall[1], Eric Kenney[2], Andreas Suter[3], Thomas Prokscha[3], Zaher Salman[3], Brian J. Kirby[4], Susanne Stemmer[1], Michael J. Graf[2] and Stephen D. Wilson[1]

High carrier density quantum wells embedded within a Mott insulating matrix present a rich arena for exploring unconventional electronic phase behavior ranging from non-Fermi-liquid transport and signatures of quantum criticality to pseudogap formation. Probing the proposed connection between unconventional magnetotransport and incipient electronic order within these quantum wells has however remained an enduring challenge due to the ultra-thin layer thicknesses required. Here we address this challenge by exploring the magnetic properties of high-density $SrTiO_3$ quantum wells embedded within the antiferromagnetic Mott insulator $SmTiO_3$ via muon spin relaxation and polarized neutron reflectometry measurements. The one electron per planar unit cell acquired by the nominal d^0 band insulator $SrTiO_3$ when embedded within a d^1 Mott $SmTiO_3$ matrix exhibits slow magnetic fluctuations that begin to freeze into a quasistatic spin state below a critical temperature T^*. The appearance of this quasistatic well magnetism coincides with the previously reported opening of a pseudogap in the tunneling spectra of high carrier density wells inside this film architecture. Our data suggest a common origin of the pseudogap phase behavior in this quantum critical oxide heterostructure with those observed in bulk Mott materials close to an antiferromagnetic instability.

npj Quantum Materials (2018)3:7 ; doi:10.1038/s41535-018-0081-8

INTRODUCTION

The origin of pseudogaps near electronic instabilities and their relationship to emergent phase behaviors in numerous transition metal oxides remains an enduring topic of research.[1,2] Though the underlying mechanisms of pseudogap formation remain debated in many compounds, canonical examples of pseudogaps in strongly correlated oxide systems often appear coincident with the partial suppression of the Mott state and the disappearance of long-range antiferromagnetism.[3,4] Pseudogaps in these systems develop below a characteristic temperature T^*, leading to the conjecture that they are the consequence of an unresolved order parameter or crossover;[5,6] however, the myriad of competing states (e.g., superconductivity,[7] charge density wave order,[8,9] spin stripe order[10]) that also arise in close proximity to the Mott phase render this connection difficult. Furthermore, the ubiquitous transition into nanoscale electronically phase separated states upon doping Mott states further blurs the unique resolution of an order parameter accompanying the pseudogap's formation.[8,11,12]

While the majority of studies begin with the Mott state and introduce carriers to access the pseudogap regime,[13–16] an alternative approach to exploring pseudogap formation is to step toward the insulating state from a weakly correlated Fermi liquid ground state. This is challenging to do under fixed disorder in bulk transition metal oxides; however thin film heterostructures with two-dimensional quantum wells provide a means of accomplishing this alternative approach. For instance, carriers can be induced within the conduction band of a d^0 layer such as $SrTiO_3$ via the creation of polar discontinuities at its bounding interfaces.[17] The induced carriers form two-dimensional electron liquids (2DELs) at each interface and the total carrier density delocalized into the $SrTiO_3$ well can be controlled by tuning the well's thickness. Correlation effects can be activated as the electron density in the well diverges,[18] and heterostructures built from $R^{3+}TiO_3/SrTiO_3$ (R = rare earth) interfaces have demonstrated that metal-insulator transitions can be driven near the thin well limit of a single SrO layer.[19]

Recent studies exploring heterostructures built from $SrTiO_3$ quantum wells embedded within a $SmTiO_3$ Mott insulating matrix have shown that, as the thin well limit is neared, $SmTiO_3/SrTiO_3$ architectures manifest an unconventional non-Fermi liquid metallic state with anomalous magnetotransport properties.[20,21] Chief among these is the appearance of a low temperature pseudogap state whose onset temperature T^* is enhanced with increasing carrier density (thinner wells).[22] The proximity of antiferromagnetism in the Mott insulating $SmTiO_3$ host matrix of this heterostructure is hypothesized to be endemic to this behavior and suggests parallels to the pseudogap states observed near the antiferromagnetic Mott states of bulk transition metal oxides.

In this paper, we report the results of a combined muon spin relaxation (μSR) and polarized neutron reflectometry (PNR) study exploring the origins of the pseudogap state in high carrier density $SmTiO_3/SrTiO_3$ quantum well heterostructures. Low energy μSR measurements capable of implanting a substantial fraction of muons within the quantum wells of this structure reveal the onset of an additional channel of muon spin damping within the T^* pseudogap phase. Precessional damping consistent with the onset of magnetic correlations within the unbound

[1]Materials Department, University of California, Santa Barbara, CA 93106, USA; [2]Department of Physics, Boston College, Chestnut Hill, MA 02467, USA; [3]Laboratory for Muon Spin Spectroscopy, Paul Scherrer Institute, CH-5232 Villigen PSI, Switzerland and [4]NIST Center for Neutron Research, National Institute of Standards and Technology, Gaithersburg, MD 20899, USA
Correspondence: Stephen D. Wilson (stephendwilson@ucsb.edu)

Received: 19 September 2017 Revised: 5 January 2018 Accepted: 18 January 2018
Published online: 20 February 2018

electron liquid residing within quantum well of this structure is observed, and polarized neutron reflectometry (PNR) measurements preclude ferromagnetic correlations as the origin of this damping. Our data demonstrate the onset of quasistatic antiferromagnetic correlations coincident with the T^* state inside the $SrTiO_3$ quantum wells and suggest that incipient antiferromagnetic order drives the formation of the pseudogap state in this oxide heterostructure.[22] More broadly, our results suggest that high density quantum wells driven towards a metal-insulator transition emulate the essential physics underlying bulk antiferromagnetic Mott states as they are destabilized via carrier substitution.

RESULTS

Low energy μSR data were collected from three thin film samples in both a weak transverse field (wTF) and under zero applied field (ZF). One sample was a 20 nm $SmTiO_3$ (SmTO) film used to observe muon depolarization arising from SmTO in the absence of proximate $SrTiO_3$ (STO). The other two samples were trilayer heterostructures containing 10 nm SmTO barrier layers bounding a $SrTiO_3$ (STO) quantum well with thicknesses of 2 and 4 nm. A 2 nm (4 nm) STO quantum well is composed of 5 SrO (10 SrO) planes alternating with 6 (11) planes of TiO_2, and all quantum well thicknesses are hereafter referenced by their number of SrO planes. Previous tunneling spectra show that in a 5 SrO quantum well a pseudogap opens at ~20 K, while a 10 SrO well does not display a gap opening above 2 K.[22]

Excellent sample quality consistent with previous reports,[23–25] including uniform layer thicknesses and sharp interfaces, was verified by measuring a reference 5 SrO quantum well heterostructure embedded between thick $SmTiO_3$ spacer layers via x-ray reflectometry measurements (Fig. 1a). Simulated muon implantation profiles for the samples above were calculated for various implantation energies with the TRIM.SP Monte Carlo code.[26] Figure 1b and c show the simulated implantation profile for 1.5 keV incident muons for the 5 SrO and SmTO control samples, respectively. This energy was found to maximize the percentage of muons landing within the STO quantum wells, resulting in nearly a quarter of all incident muons landing within the $SrTiO_3$ layer for the case of the 5 SrO thick well.

wTF μSR measurements are shown in Fig. 2 where the average time-dependent muon polarization P(t) was fit to the form $P(t) = \exp(-\lambda t)\cos(\gamma_\mu B t + \varphi)$ and where B is the local field at the muon stopping site, $\gamma_\mu = 851.6\ \mathrm{Mrad\ s^{-1}T^{-1}}$ is the muon gyromagnetic ratio, and φ is a phase constant which is determined by the detector positions relative to the initial muon spin polarization. Here the depolarization rate λ represents an average response of the muons throughout the sample volume. In wTF measurements, λ is typically dominated by dephasing between individual muon decay events due to slight variations in the static local field at the muon location.[27,28] However, λ will also increase when moment

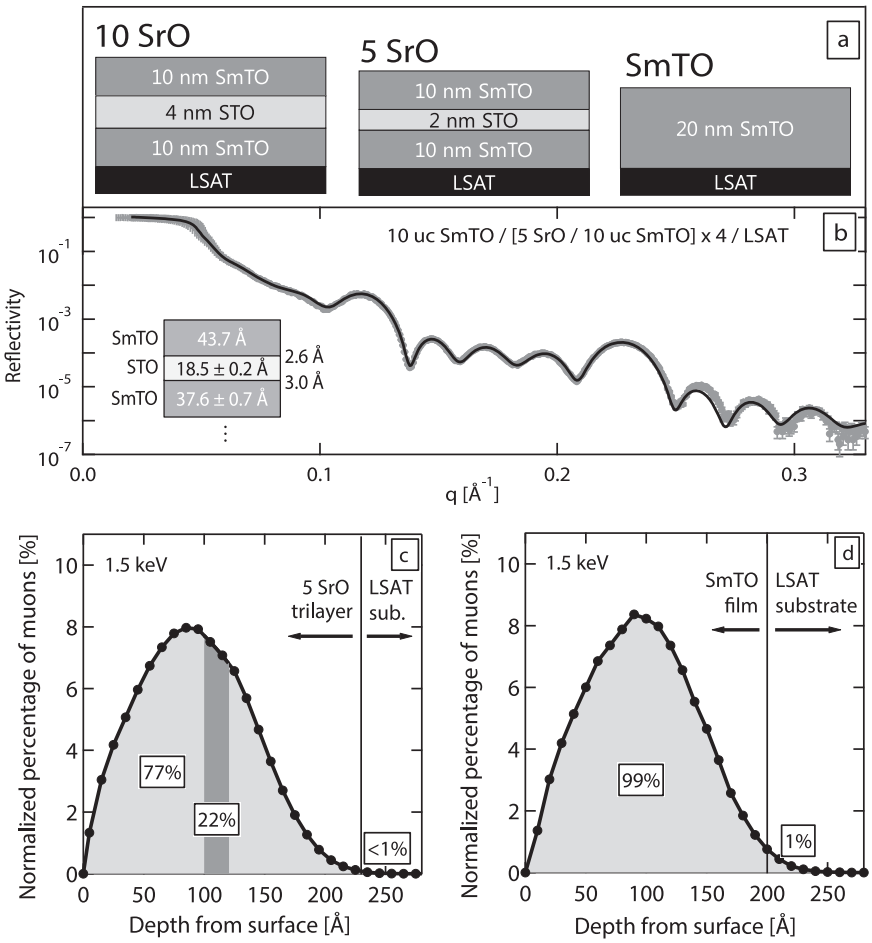

Fig. 1 X-ray reflectometry and muon implantation profiles for $SmTiO_3/SrTiO_3$ and $SmTiO_3$ films. **a** Schematic of the three samples studied via μSR. **b** X-ray reflectometry data and fit of a reference $SmTiO_3$–$SrTiO_3$ superlattice with 5 SrO thick quantum wells used to check for interface quality. Schematic inset shows the superlattice layer stack with interfacial rms (root mean square) roughness values for the top interface of each type of layer. Simulated muon implantation profiles are shown for (**c**) the 5 SrO quantum well and (**d**) the $SmTiO_3$ film, calculated using the TRIM.SP Monte Carlo code. Error bars are one standard deviation

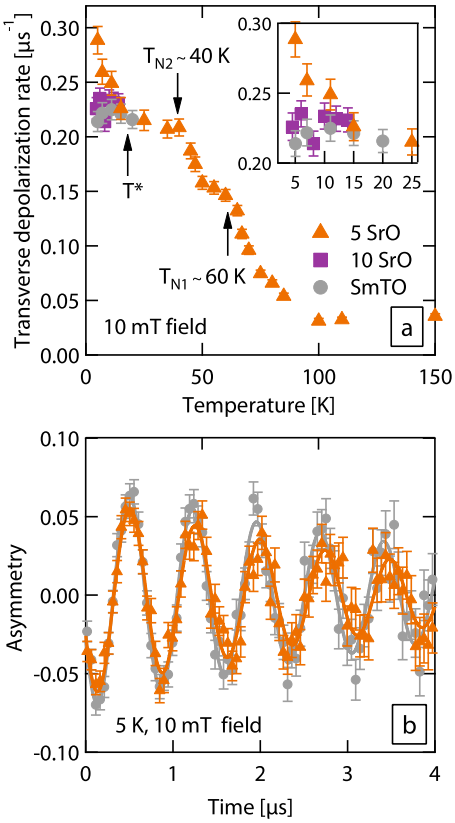

Fig. 2 Weak transverse field μSR relaxation rates and asymmetry. Temperature-dependence of the muon transverse depolarization rates (**a**) for the trilayer 5 SrO film (orange triangles), 10 SrO film (purple squares), and $SmTiO_3$ control film (gray circles) extracted from fitting weak transverse field data, as shown in (**b**) for the 5 SrO and SmTO samples at 5 K. Note that initial asymmetry values at low temperature are small due to limited t_0 resolution and a large fraction of muons depolarizing rapidly inside the magnetically ordered SmTO. Both plots use the key shown in (**a**). Error bars are one standard deviation

fluctuations slow down into the experimental range and become observable (i.e., THz → GHz). Therefore, an increase in λ for a system containing local magnetic moments can be interpreted as the slowing down of the magnetic moment fluctuation rate, which may or may not result in quasistatic order.

Figure 2a shows the temperature evolution of the transverse depolarization rate, λ, for the 5 SrO film. As the film is cooled, an initial increase in λ is observed followed by a partial saturation near the expected Neel temperature $T_{N1} = 60$ K for the Ti^{3+} sublattice in bulk SmTO. Upon further cooling, a second increase in λ followed by a partial saturation is observed at $T_{N2} = 40$ K, consistent with the expected Sm^{3+} sublattice bulk ordering temperature.[29,30] Surprisingly however, as the 5 SrO film is cooled below T_{N2}, a third, nonsaturating upturn in λ appears below 20 K.

Instead, this anomalous low temperature increase in the wTF λ suggests a third set of moments freezing, distinct from the two ordered sublattices in the SmTO layers. Further illustrating this distinction, low temperature wTF μSR measurements collected on the 10 SrO trilayer and SmTO control film are overplotted with the 5 SrO data in Fig. 2a. Importantly, no comparable low temperature upturn in λ below 20 K is observed in either sample. This demonstrates that the enhanced depolarization rate observed in the 5 SrO architecture is not inherent to SmTO, nor is it due simply to the introduction of an STO layer or STO/SmTO interfaces. Raw data demonstrating the difference in the decay envelope of

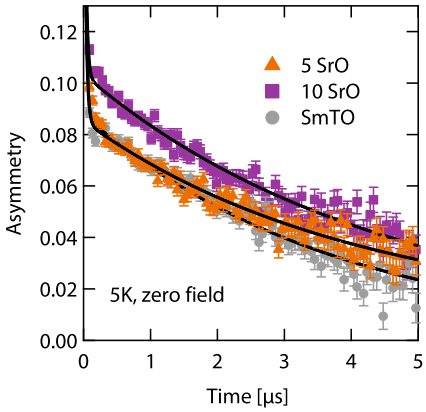

Fig. 3 Zero field μSR asymmetry. Zero field muon spin relaxation measurements of the 5 SrO film (orange triangles), 10 SrO film (purple squares), and $SmTiO_3$ control film (gray circles) at 5 K. Error bars are one standard deviation

asymmetry values P(t), from which λ is extracted, of the 5 SrO and SmTO films at 5 K are plotted Fig. 2b.

We stress that the formation of muonium, a bound state between a positive muon and an electron (μ^+e^-), cannot be the origin for this additional upturn in λ the 5 SrO data for a number of reasons. First, no upturn is observed in the 10 SrO sample, where approximately 50% of the well width is outside the extent of the interface induced 2DEL (i.e. insulating regions).[31] Second, in the case of an undoped STO film, muonium formation was previously shown to occur at 70 K,[32] far from the 20 K upturn in the trilayer wTF data. Finally, muonium formation is often suppressed in metallic materials such as STO quantum wells that contain highly confined 2DELs.[17,27]

Zero field μSR data were collected to provide further insight into the different low temperature magnetic states observed in wTF. Shown in Fig. 3 are zero field cooled, ZF μSR data collected at 5 K that have been fit to a model composed of a linear combination of two exponential functions, $P_{ZF}(t) = f*\exp\{-\lambda_{fast}\ t\} + (1\text{-}f)*\exp\{-\lambda_{slow}\ t\}$. This type of function is commonly used to capture disordered magnetic systems in which oscillations from long-range magnetic order have been overdamped.[33–35] The fast relaxation term λ_{fast} conventionally reflects muons depolarized via an inhomogeneous, static local field while the λ_{slow} term is reflective of muons depolarized via slower fluctuations.[35] The lack of ZF oscillations in the ordered state of SmTO may be attributed to these layers possessing two magnetic sublattices with similar ordered moments[30] and four-fold symmetric domains ~50–100 nm in diameter when grown on cubic LSAT substrates.[25,36] In addition, the large energy spread (~0.5 keV) of the incident muons reduces the t_0 resolution of the spectrometer.[26] Together these features make the observation of ZF oscillations unlikely, and instead λ_{fast} is determined by the nonuniformity of the internal field seen by the muons.

Relaxation rates for the fast and slow depolarization processes in the STO portion of the quantum well structures were extracted using rates measured independently from the SmTO control film to represent the 78% (70%) of the 5 (10) SrO film muon stopping sites outside of the STO well. The best fit to the SmTO data was achieved with a fast fraction of muons, $f_{fast} = 0.73 \pm 0.003$, decaying at $44.5 \pm 1.05\ \mu s^{-1}$ while the slowly decaying fraction of muons decayed at $0.26 \pm 0.005\ \mu s^{-1}$. The remaining 22% (30%) of the 5 (10) SrO film volume is described by using the same form of fast and slow relaxation terms, representing the quasistatic ordered and slow spin fluctuation contributions to the muon decay in the STO well, respectively.

The STO in the 5 SrO film had a similar fraction of fast decaying muons, $f_{fast} = 0.79 \pm 0.006$, as the pure SmTO film. This similarity

suggests two corollaries: (1) the 5 SrO film is magnetized to a similar degree as the SmTO film, a known antiferromagnet well below its Neel temperature, and (2) the entirety of the 5 SrO sample, including the entire STO quantum well, possesses these magnetic correlations, as was previously shown to be the case for STO quantum wells embedded within a $GdTiO_3$ matrix.[23] In a homogeneous or nearly ordered picture of the STO layer, this corresponds to the onset of quasistatic magnetic order with $\cos^2\Theta = 0.21$ with Θ being the angle between the muon's incident spin and the local magnetic field. In an inhomogeneous picture, the reduction in the slowly fluctuating volume fraction corresponds to slow fluctuations freezing into a distinct volume possessing quasistatic spin correlations. Both scenarios are consistent with the wTF results showing a low temperature onset of magnetic correlations in the STO layer, and ZF data suggest the lack of saturation in wTF data below 20 K as due to robust fluctuations persisting in the STO layer at 5 K.

By comparison, the fraction of fast decaying muons in the 10 SrO film was found to be only 0.57 ± 0.005. This lower fraction of fast decaying muons in the STO of the 10 SrO film explains why, at short time scales ($t < 1$ μs) in Fig. 3, the 10 SrO film has notably higher asymmetry values than either the 5 SrO or control SmTO samples. This offset arises from implanted muons that localize within a non-magnetic portion of the 10 SrO well and therefore do not undergo fast depolarization. Over longer time scales, the trends in Fig. 3 are controlled by the slowly decaying muons and their relaxation rates. The decay rates for the STO portion of the 10 and 5 SrO films both refine to be slower than the slowly decaying muons in the SmTO, 0.15 ± 0.007 and $0.08 \pm 0.014\ \mu s^{-1}$, respectively.

The low temperature enhancement of λ in the wTF measurement below $T^* \approx 20$ K and the strong fast depolarization under ZF are suggestive of magnetic moments associated with the free electrons near quantum well interfaces of the 5 SrO film. In order to probe whether these correlations carry a net magnetization and whether a field-induced response appears similar to the case of $GdTiO_3/SrTiO_3$ quantum well heterostructures, PNR measurements were performed (See Supplemental Material for additional information) on a $SmTiO_3/SrTiO_3$ superlattice film with 2 SrO thick quantum wells and 4 nm thick SmTO spacing layers. The switch from a 5 SrO to a 2 SrO thick quantum well structure was motivated by previous measurements showing a stronger magnetic response in more highly confined well structures,[23] and a field of 0.7 T (70 times larger than that utilized in wTF μSR measurements) was utilized to further maximize any potential field-induced magnetic polarization in the plane of the film.

Figure 4a shows that the PNR data collected at 4 K from the two non-spin flip channels (R^{++} and R^{--}) lie directly on top of one another, revealing no net magnetization in the plane of the film. To highlight the lack of a net magnetization, the spin asymmetry is plotted in Fig. 4b, and the nonmagnetic model fit to the data is plotted in Fig. 4c. As the antiferromagnetic structure of the SmTO layers in this superlattice has no net magnetization, this measurement is very sensitive to any potential magnetism in the STO layers. The sensitivity in this experiment is estimated to be better than 7.25 kA/m (9 mT) or roughly 0.05 μ_B per Ti ion, a value significantly smaller than the reported ordered moments for both Sm^{3+} (0.72 μ_B) and Ti^{3+} (0.43 μ_B) in $SmTiO_3$.[30] This bound is also much smaller than the value of 1 μ_B /Ti for a fully polarized state of $S = ½$ Ti^{3+} moments naively associated with free electrons in the quantum well.[23] These data preclude a picture of a low temperature, field-driven polarized state in the 5 SrO trilayer film and instead suggest that the magnetic correlations probed in μSR data are antiferromagnetic in nature.

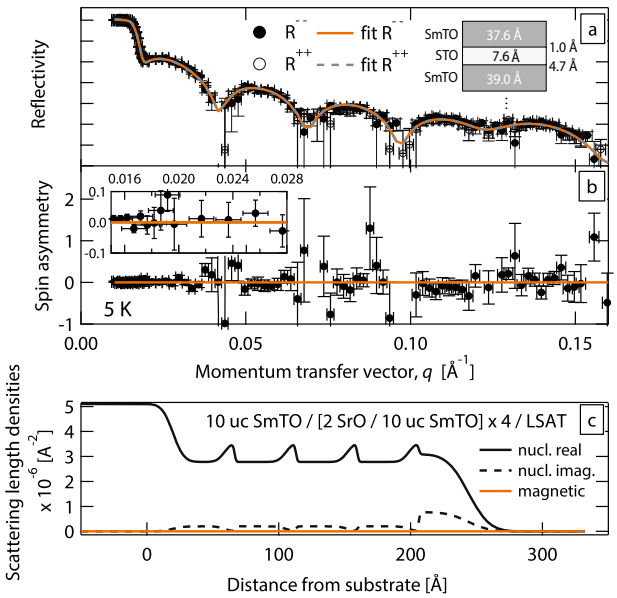

Fig. 4 Polarized neutron reflectometry data and structural model of a $SmTiO_3/SrTiO_3$ superlattice film with 2 SrO quantum wells. Panel (**a**) displays polarized neutron reflectometry data in both the R^{++} (open circles) and R^{--} (closed circles) channels. Inset shows layer structure with interfacial rms roughness given for the top of each layer type. The spin asymmetry (**b**) is calculated from PNR data in (**a**). In both (**a**) and (**b**), the best fit to the data is overlaid on the data (lines). Inset in (**b**) is a close up of the spin asymmetry over the critical edge and has the same axis units as the larger panel. The refined layer model of the superlattice (**c**) includes the real nuclear (solid black), imaginary nuclear (dashed black), and magnetic (solid orange) components of the scattering profile. Error bars are one standard deviation

DISCUSSION

Quasistatic magnetic correlations associated with the introduction of free electrons into the 5 SrO quantum well film could have a number of origins; however, data from the 10 SrO sample rule many of them out. For example, Sm^{3+} or Ti^{3+} moments localized near the well interfaces, which have not frozen/ordered due to interactions with the free electrons in the STO layers, could in theory contribute to correlations within the well electrons themselves. Alternatively, oxygen defects in STO or at the SmTO/STO interface could produce a magnetic response (See Supplemental Material for additional information). However, if either of these mechanisms were active, their signatures should have been observed in the 10 SrO sample. Furthermore, the magnetic response of trivial oxygen defects in STO is quite distinct from that observed here (See Supplemental Material for additional information). Instead, the remaining scenario consistent with our data is that the moments of the polarity-induced electrons localized within the wells themselves may undergo quasistatic freezing. In this scenario, the onset of magnetic freezing is coupled to the free carriers in the quantum wells and can naively bias the resulting charge transport through the well.

Earlier measurements of $SmTiO_3/SrTiO_3$ heterostructures have shown that at the critical well thickness of 5 SrO layers, non-Fermi liquid transport manifests and the inverse Hall coefficient (apparent carrier density) diverges, suggestive of the influence of a nearby quantum critical point.[18] The underlying order parameter driving this anomalous well transport is likely coupled to the appearance of a low temperature pseudogap in the tunneling spectra of thin well $SmTiO_3/SrTiO_3$ heterostructures. For 5 SrO thick wells, a pseudogap appears below ~20 K consistent

with the T^* freezing transition resolved in our wTF μSR data.[22] This connects the quasistatic spin freezing to the free carriers in the wells as the origin for pseudogap formation. Furthermore, the proximity of the antiferromagnetic $SmTiO_3$ host is key to stabilizing this behavior. Identical quantum well structures inside a ferrimagnetic $GdTiO_3$ host do not produce a similar pseudogap state, but rather induce ferromagnetism within the quantum wells and Fermi liquid transport.[21,22,25]

The opening of a pseudogap in high carrier density $SmTiO_3$/$SrTiO_3$ quantum well heterostructures is reminiscent of pseudogap formation in bulk transition metal oxides close to destabilized antiferromagnetic Mott states. In systems as diverse as cuprates,[3] manganites,[14] and iridates,[16] pseudogaps emerge as the Mott charge gap is quenched, yet robust short-range/fluctuating antiferromagnetic correlations remain.[37–39] Our combined μSR and PNR data point toward a model of quasistatic antiferromagnetism induced by neighboring antiferromagnetic $SmTiO_3$ layers within high carrier density $SrTiO_3$ quantum wells. The coinciding onset temperatures of antiferromagnetic fluctuations in wTF μSR measurements and pseudogap formation from earlier tunneling measurements strongly suggest that magnetic correlations in the $SrTiO_3$ quantum well constitute the origin of the pseudogap formation in this system. Our results support the notion that the essential physics for pseudogap formation in an array of doped transition metal oxides with parent antiferromagnetic Mott states is captured in high density quantum wells embedded within an antiferromagnetic Mott matrix.

METHODS

Thin film growth

$SmTiO_3$/$SrTiO_3$/$SmTiO_3$ quantum well structures and $SmTiO_3$ thin films were grown on (001) $(La_{0.3}Sr_{0.7})(Al_{0.65}Ta_{0.35})O_3$ (LSAT) substrates by hybrid molecular beam epitaxy (MBE), as described in detail elsewhere.[36,40] Both materials were co-deposited in ultra-high vacuum (i.e., ~10^{-8} Pa) on a heated substrate using elemental solid sources for Sm and Sr and a metal-organic precursor to supply Ti and O atoms. $SmTiO_3$ barrier thicknesses were nominally 10 nm thick on either side of the $SrTiO_3$ quantum well. The average quantum well thickness, which we specify by the numbers of SrO planes they contain, was controlled with single-layer precision using in-situ reflection high-energy electron diffraction (RHEED). All samples were below the critical thickness for strain relaxation as evidenced by x-ray diffraction and electron microscopy measurements on similar structures. The polar discontinuity of the $SrTiO_3$/$SmTiO_3$ interface electrostatically introduces a constant sheet carrier density of $\approx 3.4 \times 10^{14}$ cm^{-2} carriers, or 6.8×10^{14} cm^{-2} carriers per quantum well into the $SrTiO_3$.[17,18,25]

X-ray reflectivity

X-ray reflectivity data were collected at the NIST Center for Neutron Research on a Cu Kα lab source reflectometer at room temperature and in ambient conditions with a fixed divergence slit.

Muon spin rotation/relaxation (μSR)

μSR data were collected at the Low Energy Muon (LEM) spectrometer on the μE4 beamline at the Paul Scherrer Institute.[41] At LEM, high-energy spin-polarized muons are passed through a moderator of condensed inert gas turning a small fraction of the incident beam into epithermal muons (15 eV) while retaining the beam's initial polarization. The moderated muons are then reaccelerated to keV implantation energies. For all measurements in this study, an implantation energy of 1.5 keV was used as discussed in the main text (c.f. Fig. 1). At these low velocities the muon beam spot size is ~10–15 mm in diameter,[26] and in order to capture the majority of incident muons, each sample was comprised of four separate 1 cm × 1 cm films placed in a 2 × 2 grid. The samples were mounted in a flow cryostat and measured over the temperature range 5 to 150 K. The initial muon polarization was in the plane of the sample. Data were collected both under a 10 mT magnetic field applied transverse to the initial muon polarization (weak transverse field, wTF) and in zero field (ZF). Note that the current time resolution on the LEM instrument is insufficient to resolve atomic muonium frequencies at the applied wTF field. All μSR data were analyzed and fit via Musrfit.[42]

Polarized neutron reflectometry

Polarized neutron reflectometry measurements were performed on the PBR reflectometer at the NIST Center for Neutron Research with an incident wavelength of 4.75 Å. Spin polarization was selected using the critical edge of Fe/Si supermirrors in combination with Mezei spin flippers before and after the sample. Measurements were collected in a specular geometry for both non-spin flip channels. The average flipping ratio between non-spin flip and spin flip channels was 54.9. The sample chosen for the PNR measurement was field cooled in a closed-cycle He cryostat and measured under a $\mu_0 H = 0.7$ T field. Analysis was performed using the Refl1D code to that implements an optical matrix formalism to refine an input structural model of the sample.[43,44]

Data availability

The data that support the findings of this study are available from the corresponding author upon reasonable request.

ACKNOWLEDGEMENTS

S. W., R. F. N., and S. S. acknowledge support under ARO award number W911NF1410379. R. F. N. was supported in part by the National Science Foundation Graduate Research Fellowship under Grant No. 1144085.

AUTHOR CONTRIBUTIONS

R. F. N., S. S, M. J. G., and S. W. planned the experimental program. R. F. N., E. K., and M. J. G ran the muon spin relaxation measurements on a beamline maintained by A. S., T. P., and Z. S. R. F. N. and B. K. performed the neutron reflectometry experiments. R. F. N. performed the data analysis in consultation with A. S., M. J. G., and S. W., P. B. M., and S. S. grew the thin film samples for experiments. R. F. N. and S. W. wrote the manuscript.

ADDITIONAL INFORMATION

Supplementary information accompanies the paper on the *npj Quantum Materials* website (https://doi.org/10.1038/s41535-018-0081-8).

Competing interests: The authors declare no competing interests.

Publisher's note: Springer Nature remains neutral with regard to jurisdictional claims in published maps and institutional affiliations.

REFERENCES

1. Sachdev, S. Quantum criticality: competing ground states in low dimensions. *Science* **288**, 475–480 (2000).
2. Senthil, T., Balents, L., Sachdev, S., Vishwanath, A. & Fisher, M. P. Quantum criticality beyond the Landau-Ginzburg-Wilson paradigm. *Phys. Rev. B* **70**, 144407 (2004).
3. Timusk, T. & Statt, B. The pseudogap in high-temperature superconductors: an experimental survey. *Rep. Prog. Phys.* **62**, 61–121 (1999).
4. Norman, M., Pines, D. & Kallin, C. The pseudogap: friend or foe of high Tc? *Adv. Phys.* **54**, 715–733 (2005).
5. Ding, H. et al. Spectroscopic evidence for a pseudogap in the normal state of underdoped high-Tc superconductors. *Nature* **382**, 51–54 (1996).
6. Kondo, T., Khasanov, R., Takeuchi, T., Schmalian, J. & Kaminski, A. Competition between the pseudogap and superconductivity in the high-Tc copper oxides. *Nature* **457**, 296–300 (2009).
7. Kastner, M., Birgeneau, R., Shirane, G. & Endoh, Y. Magnetic, transport, and optical properties of monolayer copper oxides. *Rev. Mod. Phys.* **70**, 897–928 (1998).
8. Sipos, B. et al. From Mott state to superconductivity in 1T-TaS_2. *Nat. Mater.* **7**, 960–965 (2008).
9. Chang, J. et al. Direct observation of competition between superconductivity and charge density wave order in $YBa_2Cu_3O_{6.67}$. *Nat. Phys.* **8**, 871–876 (2012).
10. Tranquada, J. et al. Neutron-scattering study of stripe-phase order of holes and spins in $La_{1.48}Nd_{0.4}Sr_{0.12}CuO_4$. *Phys. Rev. B* **54**, 7489–7499 (1996).
11. Hogan, T. et al. First-order melting of a weak spin-orbit Mott insulator into a correlated metal. *Phys. Rev. Lett.* **114**, 257203 (2015).

12. Yee, C.-H. & Balents, L. Phase separation in doped Mott insulators. *Phys. Rev. X* **5**, 021007 (2015).
13. Lee, P. A., Nagaosa, N. & Wen, X.-G. Doping a Mott insulator: physics of high-temperature superconductivity. *Rev. Mod. Phys.* **78**, 17–85 (2006).
14. Saitoh, T. et al. Temperature-dependent pseudogaps in colossal magnetoresistive oxides. *Phys. Rev. B* **62**, 1039–1043 (2000).
15. Uchida, M. et al. Pseudogap of metallic layered nickelate $R_{(2-x)}Sr_{(x)}NiO_4$ (R = Nd, Eu) crystals measured using angle-resolved photoemission spectroscopy. *Phys. Rev. Lett.* **106**, 027001 (2011).
16. de la Torre, A. et al. Collapse of the Mott gap and emergence of a nodal liquid in lightly doped Sr_2IrO_4. *Phys. Rev. Lett.* **115**, 176402 (2015).
17. Stemmer, S. & James Allen, S. Two-dimensional electron gases at complex oxide interfaces. *Ann. Rev. Mater. Res.* **44**, 151–171 (2014).
18. Mikheev, E., Freeze, C. R., Isaac, B. J., Cain, T. A. & Stemmer, S. Separation of transport lifetimes in $SrTiO_3$-based two-dimensional electron liquids. *Phys. Rev. B* **91**, 165125 (2015).
19. Zhang, J. Y. et al. Correlation between metal-insulator transitions and structural distortions in high-electron-density $SrTiO_3$ quantum wells. *Phys. Rev. B* **89**, 075140 (2014).
20. Jackson, C. A., Zhang, J. Y., Freeze, C. R. & Stemmer, S. Quantum critical behaviour in confined $SrTiO_3$ quantum wells embedded in antiferromagnetic $SmTiO_3$. *Nat. Commun.* **5**, 4258 (2014).
21. Jackson, C. A. & Stemmer, S. Interface-induced magnetism in perovskite quantum wells. *Phys. Rev. B* **88**, 180403 (2013).
22. Marshall, P. B., Mikheev, E., Raghavan, S. & Stemmer, S. Pseudogaps and emergence of coherence in two-dimensional electron liquids in $SrTiO_3$. *Phys. Rev. Lett.* **117**, 046402 (2016).
23. Need, R. et al. Interface-driven ferromagnetism within the quantum wells of a rare earth titanate superlattice. *Phys. Rev. Lett.* **117**, 037205 (2016).
24. Zhang, J. Y., Jackson, C. A., Raghavan, S., Hwang, J. & Stemmer, S. Magnetism and local structure in low-dimensional Mott insulating $GdTiO_3$. *Phys. Rev. B* **88**, 121104 (2013).
25. Zhang, J. Y., Hwang, J., Raghavan, S. & Stemmer, S. Symmetry lowering in extreme-electron-density perovskite quantum wells. *Phys. Rev. Lett.* **110**, 256401 (2013).
26. Morenzoni, E. et al. Implantation studies of kev positive muons in thin metallic layers. *Nucl. Instrum. Meth. B* **192**, 254–266 (2002).
27. De Reotier, P. D. & Yaouanc, A. Muon spin rotation and relaxation in magnetic materials. *J. Phys. Condens. Matter* **9**, 9113–9166 (1997).
28. Maurel, L. et al. Nature of antiferromagnetic order in epitaxially strained multiferroic $SrMnO_3$ thin films. *Phys Rev. B* **92**, 024419 (2015).
29. Zhou, H. D. & Goodenough, J. B. Localized or itinerant TiO_3 electrons in $RTiO_3$ perovskites. *J. Phys. Condens. Matter* **17**, 7395–7406 (2005).
30. Amow, G., Greedan, J. & Ritter, C. An investigation of the magnetic properties of $Sm_{(1-x)}TiO_3$ for x = 0.03, 0.05, and 0.10: Magnetic structure determination of $Sm_{0.97}TiO_3$ by short-wavelength neutron diffraction on single crystals. *J. Solid State Chem.* **141**, 262–269 (1998).
31. Moetakef, P. et al. Electrostatic carrier doping of $GdTiO_3/SrTiO_3$ interfaces. *Appl. Phys. Lett.* **99**, 232116 (2011).
32. Salman, Z. et al. Direct spectroscopic observation of a shallow hydrogen-like donor state in insulating $SrTiO_3$. *Phys. Rev. Lett.* **113**, 156801 (2014).
33. Boris, A. et al. Dimensionality control of electronic phase transitions in nickel-oxide superlattices. *Science* **332**, 937–940 (2011).
34. Stilp, E. et al. Magnetic phase diagram of low-doped $La_{(2-x)}Sr_{(x)}CuO_4$ thin films studied by low-energy muon-spin rotation. *Phys. Rev. B* **88**, 064419 (2013).
35. Schneider, C. W. et al. Coexisting multiple order parameters in single-layer $LuMnO_3$ films. *Phys. Rev. B* **94**, 054423 (2016).
36. Moetakef, P., Zhang, J. Y., Raghavan, S., Kajdos, A. P. & Stemmer, S. Growth window and effect of substrate symmetry in hybrid molecular beam epitaxy of a Mott insulating rare earth titanate. *J. Vac. Sci. Technol. A.* **31**, 041503 (2013).
37. Birgeneau, R. J., Stock, C., M. Tranquada, J. & Yamada, K. Magnetic neutron scattering in hole-doped cuprate superconductors. *J. Phys. Soc. Jpn.* **75**, 111003 (2006).
38. Chen, X. et al. Influence of electron doping on the ground state of $(Sr_{(1-x)}La_{(x)})_2IrO_4$. *Phys. Rev. B* **92**, 075125 (2015).
39. Gretarsson, H. et al. Persistent paramagnons deep in the metallic phase of $Sr_{(2-x)}La_{(x)}IrO_4$. *Phys. Rev. Lett.* **117**, 107001 (2016).
40. Jalan, B., Engel-Herbert, R., Wright, N. J. & Stemmer, S. Growth of high-quality $SrTiO_3$ films using a hybrid molecular beam epitaxy approach. *J. Vac. Sci. Technol. A.* **27**, 461–464 (2009).
41. Prokscha, T. et al. The new μe4 beam at PSI: A hybrid-type large acceptance channel for the generation of a high intensity surface-muon beam. *Nucl. Instrum. Meth. A* **595**, 317–331 (2008).
42. Suter, A. & Wojek, B. Musrfit: a free platform-independent framework for μSR data analysis. *Physcs Proc.* **30**, 69–73 (2012).
43. Majkrzak, C. F. Polarized neutron reflectometry. *Phys. B* **173**, 75–88 (1991).
44. Kirby, B. J. et al. Phase-sensitive specular neutron reflectometry for imaging the nanometer scale composition depth profile of thin-film materials. *Curr. Opin. Colloid Interf Sci* **17**, 44–53 (2012).